Nano Energy 66 (2019) 104143

Contents lists available at ScienceDirect

Nano Energy

journal homepage: http://www.elsevier.com/locate/nanoen

Full paper

Stretchable conductive nonwoven fabrics with self-cleaning capability for tunable wearable strain sensor

Hu Liu [a,*], Qianming Li [a], Yibing Bu [a], Na Zhang [a], Chunfeng Wang [a,b], Caofeng Pan [b,**], Liwei Mi [c], Zhanhu Guo [d], Chuntai Liu [a,***], Changyu Shen [a]

[a] Key Laboratory of Materials Processing and Mold (Zhengzhou University), Ministry of Education, National Engineering Research Center for Advanced Polymer Processing Technology, Zhengzhou University, Zhengzhou, Henan, 450002, China
[b] Beijing Institute of Nanoenergy and Nanosystems, Chinese Academy of Sciences, National Center for Nanoscience and Technology (NCNST), Beijing, 100083, China
[c] School of Materials and Chemical Engineering, Zhongyuan University of Technology, Zhengzhou, Henan, 451191, China
[d] Integrated Composites Laboratory (ICL), Department of Chemical & Biomolecular Engineering, University of Tennessee, Knoxville, TN, 37996, United States

ARTICLE INFO

Keywords:
Non-woven fabrics
Strain sensor
Micro-crack
Superhydrophobic
Self-cleaning

ABSTRACT

With the fast growth of wearable intelligent devices, tunable strain sensors with broad strain sensing range and high sensitivity are in urgent demand. Furthermore, the merits of excellent waterproof property, self-cleaning, and anti-corrosion are also imperative for the practical applications of them. Herein, a tunable wearable micro-cracked non-woven fabrics (NWF) strain sensor with broad strain sensing range and high sensitivity was successfully developed based on the electrically conductive cellulose nanocrystal (CNC)/graphene (G) coating with controllable micro-crack density, which was achieved through changing the G loading of the coating layer, and its superhydrophobicity was achieved by simply dip-coating in the hydrophobic fumed silica (Hf-SiO_2)/ethanol dispersion. As a result, a broad working range of 98% and GF value up to 2.36×10^4 are simultaneously achieved for the prepared strain sensor (G content is 25 wt%). In addition, it possesses an ultralow detection limit as low as 0.1%, short response time (33 ms) and good sensing stability over 1000 cycles. What's more, the NWF strain sensor presents excellent waterproofness (WCA = 154°), anti-corrosion ability, outstanding self-cleaning and stability. Due to the excellent response performances, the NWF strain sensor can successfully monitor various human activities from subtle deformations (e.g. speech recognition, pulse waves) to vigorous body movements (e.g. finger, elbow joint and wrist movement). Specially, owing to its excellent superhydrophobic characteristic, the strain sensor also exhibits superior self-cleaning capability and good applicability in a humid or underwater harsh outdoor environment.

1. Introduction

With the fast growth of wearable intelligent devices, wearable and stretchable strain sensors have aroused tremendous interests in many fields, such as E-skin [1–3], human-machine interfaces [4–6], human health detection [7–10], smart robotics [11–13], and structure health monitoring [14,15]. Generally, broad strain sensing range (>50%) and high sensitivity (gauge factor (GF) > 100) are the two crucial indexes needed to be considered for the design of wearable strain sensors to monitor both of the subtle deformations (e.g., human voice recognition, pulse, swallowing, and heartbeat) and the large deformations (e.g., elbow joint, knee joint, and finger movement) [14,16]. However, it is still an enormous challenge to achieve the simultaneous enhancement of them [17–20]. Furthermore, the merits of tunable sensing property, low-cost, and scalable fabrication are also imperative characteristics needed to be considered for ideal wearable strain sensors.

To meet these requirements, polymer composites that are consisted of the stretchable elastic polymer (e.g., such as TPU, PDMS, SEBS, and rubber) and highly electrically conductive nanofiller (e.g., CB, CNT, graphene, Mxene, and CNF) have been widely investigated [14,21–30]. For example, Yu et al. prepared the PDMS based strain sensor through coating the conductive CNT layer on its surface, showing a 400% sensing

* Corresponding author.
** Corresponding author.
*** Corresponding author.
E-mail addresses: liuhu@zzu.edu.cn (H. Liu), cfpan@binn.cas.cn (C. Pan), ctliu@zzu.edu.cn (C. Liu).

https://doi.org/10.1016/j.nanoen.2019.104143
Received 18 August 2019; Received in revised form 22 September 2019; Accepted 27 September 2019
Available online 1 October 2019

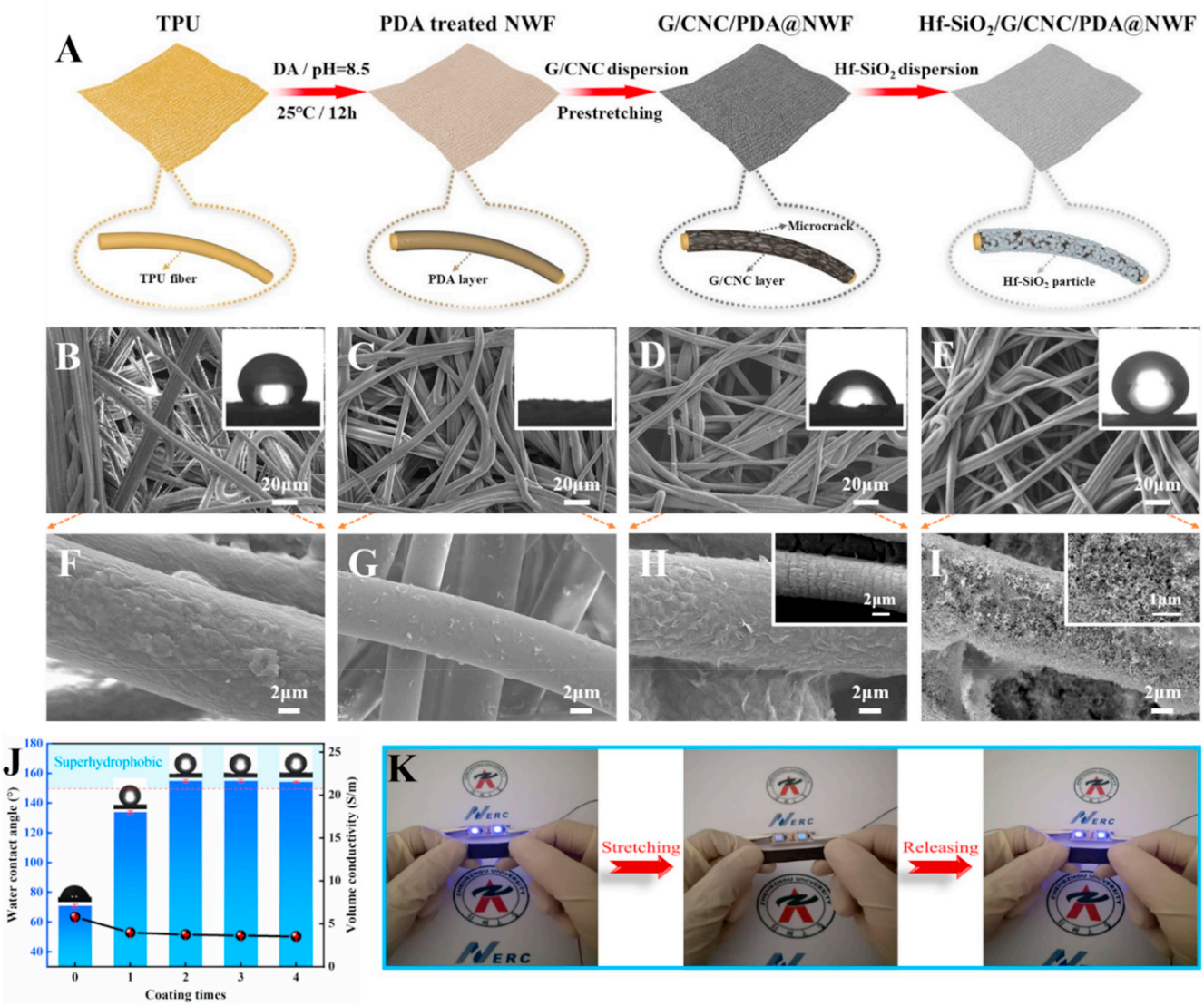

Fig. 1. Structure and electrical property of the Hf-SiO_2/G/CNC/PDA@NWF composites. (A) Schematic preparation of Hf-SiO_2/G/CNC/PDA@NWF composites. Surface SEM images of the surface of (B&F) original NWF, (C&G) PDA@NWF, (D&H) G/CNC/PDA@NWF and (E&I) Hf-SiO_2/G/CNC/PDA@NWF. Insets are the optical photographs of WCA. (J) WCA and conductivity of the Hf-SiO_2/G/CNC/PDA@NWF composites treated with different coating times in Hf-SiO_2 suspension. Insets are the optical photographs of WCA. (K) Photographs of a LED connected with the Hf-SiO_2/G/CNC/PDA@NWF composites, showing the light intensity variation under the external stretching and release.

range but a low GF of 0.2 [19]. Liu et al. developed the porous graphene/TPU strain sensor using the solution blending and freeze drying techniques. It exhibited a broad strain range (up to 90%), yet the sensitivity was relatively low (GF = 1.2) [31]. Additionally, strain sensors with special geometrical structures (e.g., microarrays, gaps and islands structures, micro-crack structure, percolation networks, wrinkled structure, and porous structure) are also widely designed to improve the sensing performances [32–39]. For instance, Wang et al. fabricated an ultrasensitive strain sensor by coating the metal thin film with micro-cracked structure on the PDMS substrate, and the sensor sensitivity is up to 5000 but working strain ranges <1% [40]. Recently, Shi et al. developed a crack-based AgNW/GO/C60@PU strain sensor through the screen-printing process, achieving the high sensitivity and broad working range (GF value up to 2392, and $\varepsilon = 62\%$) simultaneously [16]. However, the complicated processing technique will no doubt restrict its cost and large-scale fabrication. Therefore, new simple but effective measures are in urgent demand for the preparation of tunable strain sensors with broad strain sensing range and high sensitivity.

Meanwhile, another issue of the wearable strain sensors is the waterproof property, which will endow the strain sensor with excellent self-cleaning and anticorrosion performances towards harsh outdoor conditions such as humid, stain, ultraviolet radiation, acid/alkaline environment [41–44]. To achieve this goal, constructing strain sensor with superhydrophobic surface was considered to be an effective strategy [45–47]. For example, Li et al. developed a CNTs/SEBS superhydrophobic smart strain sensor by preparing the micrometer-sized pit-like structure on its surface, and the waterproofness and chemical stability of the sensor was significantly enhanced [42]. Similarly, Wang et al. also prepared a superhydrophobic strain sensor with improved sensing stability and anti-corrosion property by partially embedding perfluorosilane-coated graphene into TPU [47]. All these make strain sensor with superhydrophobic surface a research hotpot.

Given the aforementioned challenges, a tunable wearable nonwoven fabrics (NWF) strain sensor with broad sensing range and high sensitivity was successfully developed based on the electrically conductive cellulose nanocrystal (CNC)/graphene (G) coating with controllable micro-crack density through the simple dip-coating and

pre-strain technique, and the superhydrophobicity of the sensor was then easily obtained by dip-coating in the Hf-SiO_2/ethanol dispersion. In addition, the effect of G loading in the conductive coating on the electromechanical properties of the sensor was systematically studied, and the developed strain sensor (G content is 25 wt%) exhibited high sensitivity (GF up to 23600), broad and tunable sensing range (ε up to 98%), ultralow detection limit as low as 0.1%, short response time (33 ms) and excellent sensing stability (over 1000 cycles). What's more, the obtained superhydrophobic sensor presents excellent waterproofness (WCA = 154°), anti-corrosion ability, outstanding self-cleaning and stability. Due to its superior sensing performances, the sensor can successfully detection a full range of human activity (tiny strain of pulse waves and speech; and vigorous body movements of finger, elbow joint and wrist movement). More importantly, the sensor can clearly detection an index finger bends in the water, the loading of the tiny water droplet and the ultrasonic wave in water, showing the excellent sensing capability in a humid or underwater environment. Overall, the superhydrophobicity of the NWF strain sensor supplies a promising chance to use in various harsh outdoor environments.

2. Experimental

2.1. Materials and chemicals

Thermoplastic polyurethane (TPU) non-woven fabrics (NWF, 110 g/m^2) was produced by the Pinghu Zhanpeng Hot Melt Film Co., Ltd. *Tris* (hydroxymethyl-amino-methane) (Tris) and dopamine hydrochloride (DA) (analytical grade) were all were supplied by Macklin Biochemical Co., Ltd. (Shanghai, China). Analytical grade Anhydrous ethanol produced by Fuyu Fine Chemical Co., Ltd. (Tianjin, China) was used without further purification. Cellulose nanocrystal (CNC) aqueous dispersion (1 wt%) was obtained from Qihong Technology Co., Ltd. (Guilin, China). Graphene (denoted as G) with a thickness of 0.55–3.74 nm and a diameter of 0.5–3 mm was obtained from Chengdu Organic Chemicals Co. Ltd., Chinese Academy of Sciences. Hydrophobic fumed silica (denoted as Hf-SiO_2, diameter: 16 nm, carbon content: 0.9 wt%, specific surface area: 110 m^2/g) was purchased from Evonik Industries Co. Ltd., Germany.

2.2. Preparation of the Hf-SiO_2/G/CNC/PDA@NWF composites

The schematic preparation of the Hf-SiO_2/G/CNC/PDA@NWF composites is illustrated in Fig. 1A. NWF was first treated in the DA/Tris buffer solution (1.4 mg/mL) with a PH value of about 8.5 under magnetic stirring at 25 °C for 12 h to get the polydopamine modified NWF (PDA@NWF), which was then washed by excess deionized water for several times to remove the residual reactants, followed by drying in an oven at 60 °C for 1 h. After that, homogeneous G/CNC aqueous dispersion (Fig. S1) was obtained through adding G into the dilute CNC aqueous dispersion (4.5 mg/mL) under sonication for 20 min (200 W). In this study, a series of G/CNC aqueous dispersions with five different G weight ratios (10%, 20%, 25%, 30% and 40%) were configured. Subsequently, PDA@NWF was dipped into the G/CNC aqueous dispersion under sonication for 20 min to obtain the conductive G/CNC/PDA@NWF composites. After drying in an oven at 60 °C, it was pre-stretched to the non-conductive state and then released at a rate of 1 mm/min to produce the microcrack structure on the fiber surface using the universal testing machine, aiming to enhance its sensitivity. Finally, the microcracked G/CNC/PDA@NWF composites were transferred into the Hf-SiO_2 ethanol dispersion (0.1 g/mL, see Table S1 for details) under ultrasonication for 10 min and dried in an oven at 60 °C for 1 h to endow the composites with superhydrophobicity. As a result, the designed Hf-SiO_2/G/CNC/PDA@NWF composites were successfully fabricated.

2.3. Characterization

The morphology and microstructure of NWF and its composites were observed using the JEOL JSM-7500F scanning electron microscopy at of 5 kV after sputter coating with gold. Water contact angles (WCAs) of NWF and its composites were tested through dropping 5 μL water droplet onto their surfaces using the SL200KS optical contact angle meter at ambient temperature. WCAs at more than five different positions were measured to obtain the average WCA. Raman spectra in the range of 400–4000 cm^{-1} was measured at room temperature using the confocal Raman spectroscopy (LabRAM HR Evolution). Fourier-transform infrared spectroscopy (FT-IR) spectrum in the range of 500–4000 cm^{-1} was recorded with a resolution of 4 cm^{-1} in the attenuated total reflectance mode (Nicolet Nexus 870).

The strain sensor was fabricated by cutting the Hf-SiO_2/G/CNC/PDA@NWF composites into rectangular samples with a dimension of $3 \times 1 \times 0.3$ mm^3 and then adhering the conductive tapes onto its the two ends as electrodes. To demonstrate the feasibility of the sample as a wearable strain sensor, the sensor was mounted onto the different parts of the body using a transparent breathable medical tape for detecting human bodily motion. Their volume resistance (R) were tested by utilizing the digital multimeter (Tektronix DMM4050), and the volume conductivity (σ) was obtained according to the formula of $\sigma = L/RS$. Here, S and L represent the cross-sectional area and distance between the electrodes of the sensor, respectively. The electromechanical behaviors of the sensor were recorded by the conjunction of a digital multimeter and a universal testing machine (SHIMADZU, Japan) (Fig. S2). Electrochemical workstation (A RST5000) was applied to investigate the response time and the current–voltage (I–V) characteristics of the sensor. Five specimens were used for each test in this work to ensure the robustness of the data.

3. Results and discussions

As shown in the SEM morphologies of the original NWF in Fig. 1B&F, it exhibits a spider's web-like structure where the rough fibers connected with each other, which is well maintained during the whole preparation process (Fig. 1C–E). The original NWF is hydrophobic in nature with a WCA of about 120° (inset in Fig. 1B). To enable the fully penetration of the G/CNC aqueous suspension into the interconnected fibrous networks subsequently, it was transferred into hydrophilic by coating a layer of PDA achieved through the self-polymerization of DA [48]. As a result, NWF color changes from light yellow to gray (Fig. S3), and the WCA of PDA@NWF was reduced to be 0° (inset in Fig. 1C), showing its superhydrophilicity (Video S1). In addition, the fiber surface turns to be smoother than that of the original NWF due to the existence of PDA (Fig. 1G). Here, the instinct adhesion of PDA and the hydrogen bonding between PDA and NWF inferred from the blue-shift of the N–H group shown in Fig. S4 A & B enables a tough interfacial bonding between them. After coating with the G/CNC layer homogeneously evidenced by the Raman spectroscopy shown in Fig. S4C, the surface of the fiber turns to be became rough due to the existence of wrinkled graphene nanosheet, and its color also changes from gray to black (Fig. 1H & Fig. S3). Then, the designed microcracks are successfully constructed through the pre-strain treatment due to difference of modulus of the G/CNC layer and NWF (insect in Fig. 1H), and the G/CNC/PDA@NWF exhibits the hydrophilic state with a WCA of 73° (inset in Fig. 1D). Finally, a layer of Hf-SiO_2 is uniformly and tightly anchored onto the TPU fibers (Fig. 1I & Fig. S4D), making them superhydrophobicity with a WCA of 155° (inset in Fig. 1E & Video S2) due to the instinct low surface energy and rough microtopography of the Hf-SiO_2 layer [49,50].

Supplementary data related to this article can be found at https://doi.org/10.1016/j.nanoen.2019.104143.

The morphology and electrical property of the G/CNC/PDA@NWF composites with different graphene loading in the G/CNC layer are shown in Fig. S5. Obviously, all samples were covered with the

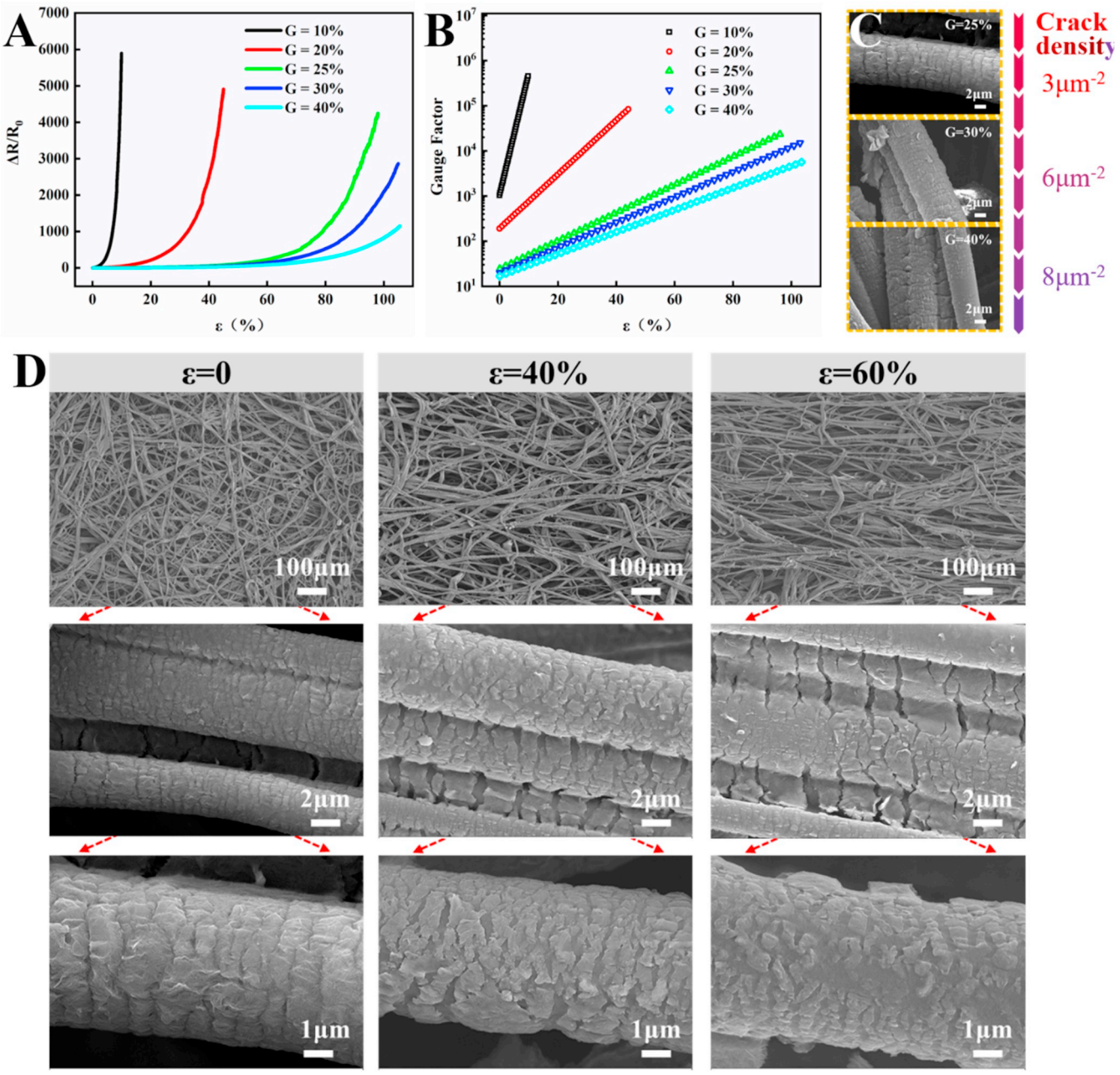

Fig. 2. Tunable microcrack structure and the sensing mechanism of the sensor. (A) $\Delta R/R_0$ and (B) GF as a function of tensile strain for the G/CNC/PDA@NWF composites with different G loading. (C) Surface SEM images of the G/CNC/PDA@NWF composites with different G loading. (D) SEM images showing the sensing mechanism of the micro-cracked stain sensor with 25% G loading.

conductive coating and the conductivity could be effectively adjusted by tuning the G loading. Fig. 1J displays the effect of the coating number in Hf-SiO_2 suspension on the conductivity and WCA of Hf-SiO_2/G/CNC/PDA@NWF composites with 25 wt% loading. The WCA increases rapidly from 73° to 153° after coating two times and then tends to be stable with further increase of the coating time, implying a limitation is reached. Meanwhile, the conductivity exhibits a slight decrease, showing that the Hf-SiO_2 layer has little influence on the conductive network of the composites. Fig. 1K shows the light intensity variation of a LED light connected with the Hf-SiO_2/G/CNC/PDA@NWF composites, in which the LED becomes darker upon external stretching based on the destruction of the conductive network and recovers to its initial intensity after release (Video S3) corresponding to the recovery of the destructed conductive network, demonstrating the great potential of the Hf-SiO_2/G/CNC/PDA@NWF composites to be used as an ideal strain sensor.

Supplementary data related to this article can be found at https://doi.org/10.1016/j.nanoen.2019.104143.

Generally, tunable sensing range and sensitivity are crucial indexes for high-performance strain sensor. As seen in Fig. 2A, the sensing range can be tuned hugely by controlling the G loading. Specially, the strain sensing range increases from 10% for 10% G loading to 45% and 98% for 20% and 25% G loading, respectively, and then slightly rises to 105% for both 30% and 40% G loading, which is limited by the elongation at break of the TPU NWF (Fig. S6). Besides, the relative resistance variation $\Delta R/R_0$ ($\Delta R = R\text{-}R_0$, where R and R_0 represent the resistance in the tensile state, and the initial resistance, respectively) increases with increasing strain for all the NWF composites, and a lower G loading produces higher sensitivity, as illustrated by the slope coefficient of the $\Delta R/R_0$–strain curve. Here, gauge factor (GF, $GF=(\Delta R/R_0)/\varepsilon$, where ε represents the applied tensile strain) is also applied to evaluate the

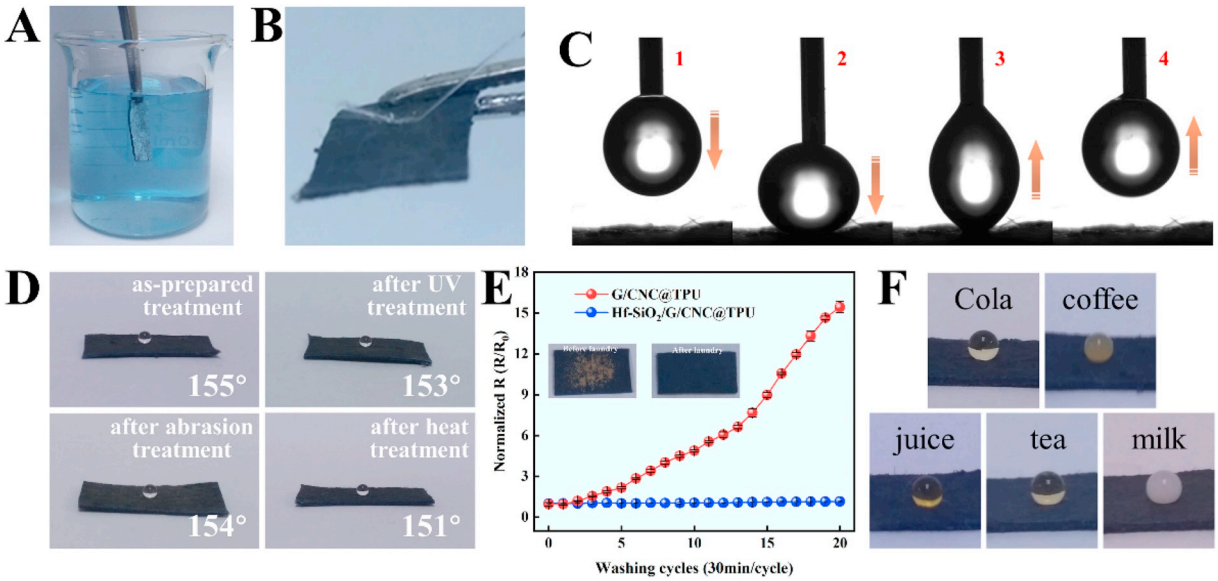

Fig. 3. Anti-corrosion and self-cleaning property of the micro-cracked NWF strain sensor. Photographs of (A) the sensor immersed in water and (B) a jetting of water bouncing off it. (C) Photographs showing the non-adhesion property of the sensor. (D) Photographs showing the WCA variation of the sensor after being treated under different environments. (E) Resistance change of the strain sensor with and without Hf-SiO_2 depending on repeated washing cycles. Insets: Photographs showing washable property of the sensor, left side: before laundry, right side: after laundry. (F) Photographs showing the state of different droplets on the superhydrophobic surface of the strain sensor.

sensitivity of the sensor. As seen in Fig. 2B, all the GFs increase linearly with the increased strain, contributing to an easy read during the data processing procedure. Especially, the GF for 10% G loading increased from 1027 at the beginning of deformation to 452600 at 10% strain, and the GF decreases with the increased G loading. However, the sensor still exhibits a GF value as high as 5600 at 105% strain for 40% G loading. The G loading dependent sensing range and sensitivity is closely associated with the microstructure formed in the G/CNC conductive layer after the pre-strain treatment. Clearly, the fiber surfaces are covered with discontinuous G/CNC layer and almost no obvious change is observed for the NWF composites with lower G loading (10% and 20%) (Fig. S7). However, as shown in Fig. 2C, a compact layer of G/CNC with typical microcrack structure is produced companying with the increased crack density (the number of discontinuous cracks per unit area) with increasing G loading from 25% to 40%. Here, the produced homogeneous microcrack is mainly ascribed to the excellent bonding between the G/CNC layer and elastomeric fiber which makes a good compliance between them, resulting an effective suppression for the strain localization of G/CNC layer and generating homogeneous microcrack upon external stress. In addition, the modulus deviation between G/CNC layer and elastomeric fiber is also reduced with the increase of G loading, leading to an increased compliance between them and larger crack density. Based on the microstructure of the fiber surface, it can be easily understood the deduction as illustrated in Fig. S8 that the connection of adjacent fibers determines the electrical conductivity of the sensor with lower G loading (10% and 20%) due to the discontinuous conductive network along the fiber, and the separation of the connected fibers upon deformation will undoubtedly induce significant resistance variation and invalidity upon small strain, causing high GF and small sensing range. For the ones with the high G loading (25%, 30% and 40%), the sensing behavior is mainly ascribed to the evolution of the microcrack structure upon tensile strain. As shown in Fig. 2D, the relaxed fibers are gradually extended along the drawing direction companying with the gradual crack propagation. Notably, the crack first gets larger and then develops into isolated strip with increasing strain from 0% to 60%. As a result, sensor with larger crack density generates lower GF and larger sensing range.

The strain sensor with the attributes of anti-corrosion and self-cleaning will be critical for their practical applications in the fields of portable devices, smart sensor systems and wearable electronics. As seen in Fig. 3A, the micro-cracked NWF strain sensor displays strong light reflection when immersed into the water due to the fact that the trapped air layer on the surface lead to the total light reflectance, resulting in the protection of the NWF strain sensor from being wetted effectively. Besides, a stream of water could bounce off the surface without leaving any residue (Fig. 3B). All these indicated that the superhydrophobicity of the sensor is successfully obtained through the simple coating technique in Hf-SiO_2 suspension, avoiding the complicated process, noxious reagent and high-cost applied in previous publications [51–54]. Furthermore, its non-adhesion property against water was also tested, Fig. 3C. Clearly, the water droplet cannot infiltrate the material even if it is forced onto the surface of the sensor, and there is no trace of water remaining on the surface after the syringe needle leaves the surface, demonstrating very weak adhesion force between them. Considering the harsh outdoor environment in practical applications, the anti-corrosion ability of the NWF strain sensor is evaluated after being exposed to UV-B radiation for 48 h, water erosion for 20 min and 100 °C heat treatment for 48 h, respectively. As a result, the WCA decreases slightly to 153°, 154° and 151° (Fig. 3D), showing stable superhydrophobicity. In addition, as shown in Fig. S9, all the samples retain their superhydrophobicity (WCA>150°) towards different pH solutions, indicating the pH value has little effect on the superhydrophobicity. What's more, washing durability is also critical for the successive use of contaminated textile materials. It can be clearly observed that the contaminated sensor turned to be spotless after being cleaned in soapy water for 30 min under magnetic stirring (about 800 r/min) (inset in Fig. 3E), and the resistance of the superhydrophobic NWF kept almost unchanged during 20 washing cycles, showing greater stability than the one without Hf-SiO_2. Finally, the superhydrophobic NWF exhibits outstanding self-cleaning (Fig. S10 & Video S4) and great repellency property towards common liquid foods, including cola, coffee, orange juice, tea and milk (Fig. 3F), where the liquids food appears to be spherical on the surface and roll off quickly without leaving any trace.

Supplementary data related to this article can be found at https://doi.org/10.1016/j.nanoen.2019.104143.

Here, the strain sensing performances of the micro-cracked NWF

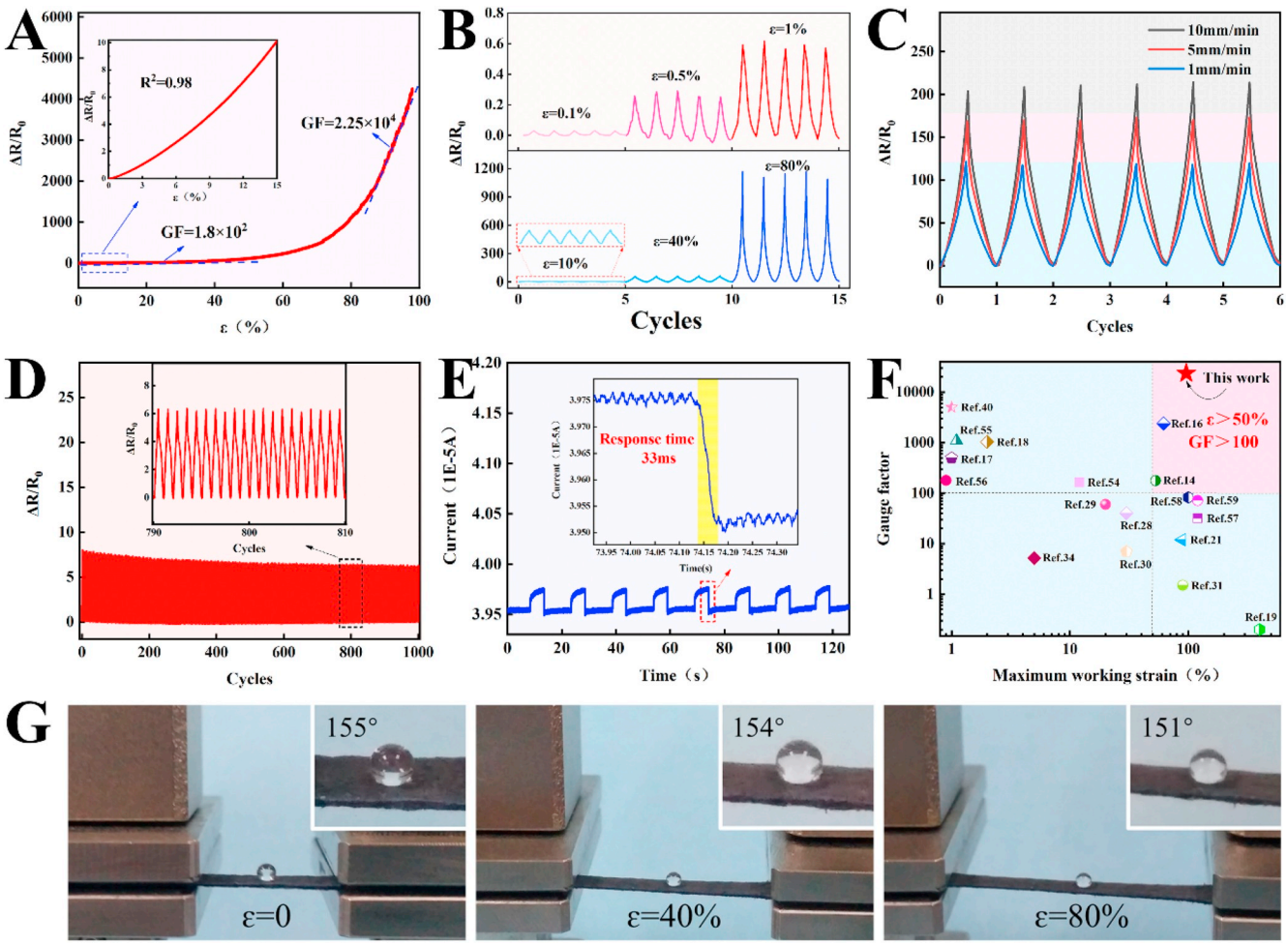

Fig. 4. Strain sensing performances of the micro-cracked NWF strain sensor. (A) $\Delta R/R_0$ as a function of strain at a tensile rate of 1 mm/min. Cyclic sensing behaviors of the sensor under (B) different tensile strain levels and (C) different tensile rates in 50% strain range. (D) Stability testing of the sensor over 1000 cycles in 10% strain range at a tensile rate of 10 mm/min. (E) The response time of the strain sensor. (F) Comparison of the maximum working range and GF of the sensor in previous publications. (G) Photographs showing the states of the water droplets on the surface of the sensor upon different tensile strains after 1000 cycles.

strain sensor with 25% G loading were systematically studied due to its high sensitivity and broad working range discussed above. Fig. 4A displays the relationship between the $\Delta R/R_0$ and strain of the sensor at a stretching rate of 1 mm/min. Obviously, the sensor exhibits a linear response to a strain up to 15% with a GF of about 180 (Video S5). Then, GF increases exponentially and reaches up to be about 23600 at 98% strain. Fig. 4B displays the strain sensing behaviors of the sensor under cyclic loadings at different strain levels, and the value of $\Delta R/R_0$ increases with increasing strain and then gradually decreases to its initial value upon releasing the strain in each cycle, showing great recoverability. In addition, the maximum value of $\Delta R/R_0$ also increases with increasing the maximum strain in the strain range of 0.1%–80%. Notably, a 0.1% tensile strain also could be e accurately detected, showing an ultralow detection limit. Similarly, as depicted in Fig. 4C, $\Delta R/R_0$ also exhibits a larger value under higher tension rate due the fact that a higher tension rate leads to larger stress, causing more serious effect on the conductive network (Fig. S11). To further explore the durability of the NWF strain sensor, 1000 tensile cycles with a 10% strain at a strain rate of 10 mm/min was conducted, Fig. 4D. As a result, the resistance varies periodically and no apparent fluctuation of each cycle is observed, verifying the good durability and stability of the sensor. What's more, the sensor possesses a response time of only 33 ms (Fig. 4E), which is much faster than the reported value of 60–300 ms [22,26,55–57]. Fig. 4F summarizes the maximum working strain range versus the GF in of various recent publication. Generally, it is difficult to strike a balance between broad working range and high sensitivity for most flexible strain sensors, as shown in the blue-colored region. For instance, most noble metallic or carbon-based flexible sensors show large GF value, however, their working ranges are very limited due to the difficulty in keeping the structure integrity for materials upon large strain [17,18,40,58–60]. In contrast, broad working range of 400% has been achieved by using the highly elastic substrate, but the GF is as low as 0.2 arising from the insignificant structural change under tiny strain [19,21,31,61–63]. Therefore, it is a great challenge for the realization of the strain sensors with both broad working range ($\varepsilon > 50\%$) and high sensitivity ($GF > 100$) simultaneously. In this work, the superhydrophobic micro-cracked NWF strain could achieve a large elongation of 98% and GF value up to 2.25×10^4 simultaneously as shown in the red region. As far as we know, they are the highest values ever reported. Finally, the stability of the superhydrophobicity of the sensor was verified after the 1000 cyclic loading. Interesting, the sensor still remained superhydrophobic under long-term use (155°/0% strain → 154°/40% strain → 151°/80% strain), showing excellent stability of the superhydrophobicity (Fig. 4G & Video S6).

Supplementary data related to this article can be found at https://doi.org/10.1016/j.nanoen.2019.104143.

Based on the high sensitivity, broad stretching range, short response time, and outstanding waterproof property of the micro-cracked NWF strain sensor, it could be applied for the full range strain signal detection, including the large-scale (such as the bending of fingers, wrists and

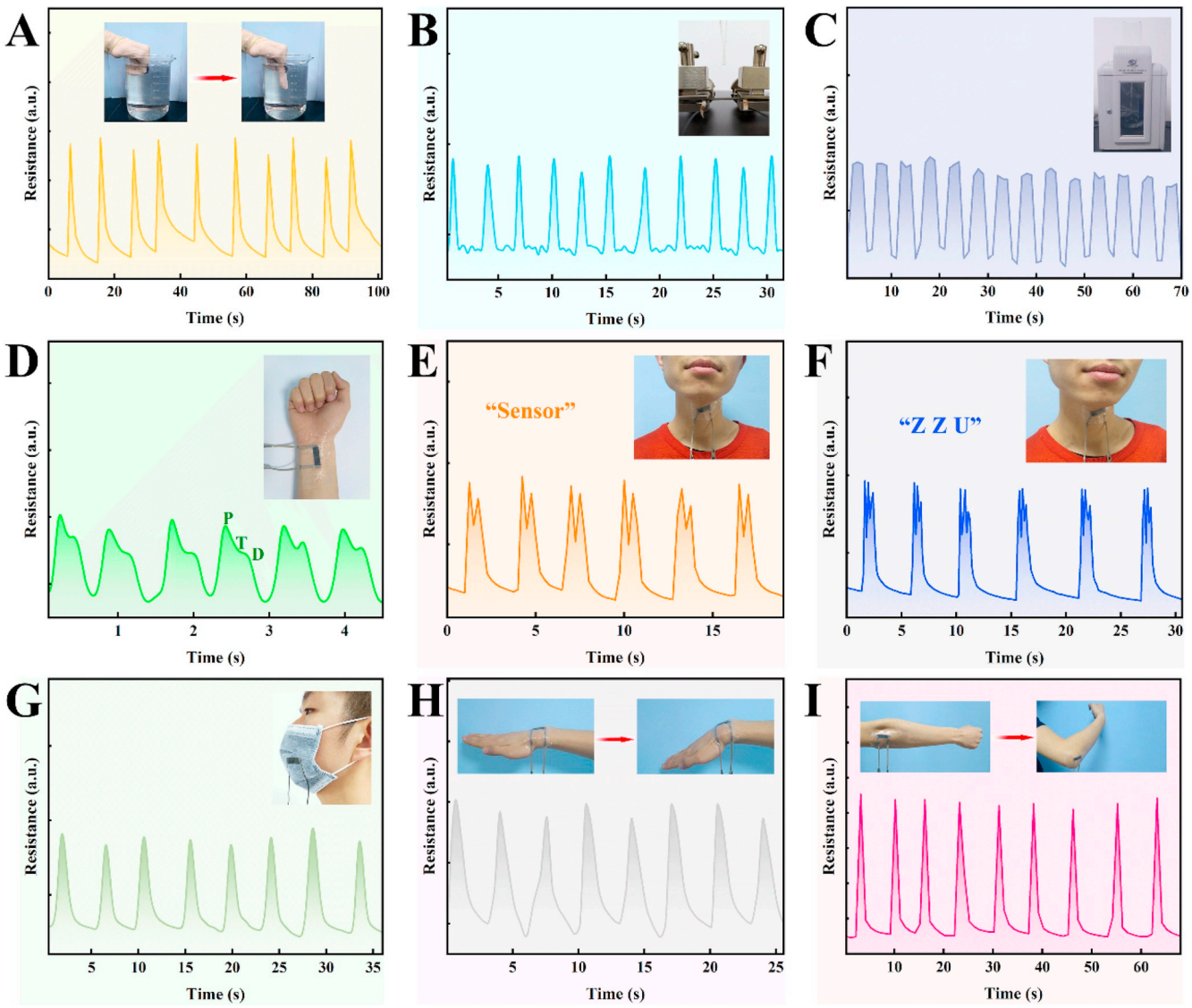

Fig. 5. Application of the micro-cracked NWF strain sensor for the real-time detection of various external strain. Resistance sensing signals of the sensor towards (A) the movement of index finger in the water, (B) a water droplet of about 0.05 mL and (C) the ultrasonic wave in water, showing the sensing capability of the sensor in a humid or underwater environment. Resistance sensing signals induced by (D) the wrist pulse, (E)&(F) pronunciation and (G) respiration. (H) and (I) Resistance sensing signals of the sensor during elbow joint and wrist movement.

arms) and small-scale (such as pulse, ultrasonic wave and voice recognition) strain change. Firstly, a smart glove was fabricated by attaching the sensor onto the glove and applied for the motion detection of an index finger in the water, Fig. 5A & Video S7. The resistance exhibits regular variation when the index finger bends repeatedly in the water. Besides, significant resistance sensing signals can also be easily obtained upon the loading of about 0.05 mL water and the ultrasonic wave in water (Fig. 5B&C, Video S8). All these indicates the excellent sensing capability of the sensor in humid or underwater environments. Meanwhile, its application as a wearable diagnostic device was also demonstrated by attaching the sensor onto the wrist, achieving the real-time monitor of the wrist pulse. As shown in Fig. 5D, three typical peaks, which are corresponded to the percussion wave (P), tidal wave (T), and diastolic wave (D), are successfully observed, and the beat rate is about 78 per minute. Interestingly, speech acquisition and recognition were also successfully achieved using the NWF sensor. As shown in Fig. 5E&F, when the volunteer says a disyllabic word "sensor" and a polysyllabic word "ZZU", the sensor attached on the volunteer's neck generated the typical two and three peaks in signal response curves, respectively, implying the huge potential of the sensor in voice recognition. What's more, the sensor can also be used for the real-time monitor of the respiration signal, elbow joint and wrist movement, showing the stable and repeatable resistance variation signal (Fig. 5G, H & I). All the testing results implied the superhydrophobic sensor could meet the various needs in practical applications.

Supplementary data related to this article can be found at https://doi.org/10.1016/j.nanoen.2019.104143.

4. Conclusion

In summary, the micro-cracked NWF strain sensor with broad working range and high sensitivity simultaneously was successfully fabricated by the simple dip-coating and pre-strain technique. Here, the designed microcrack structure was constructed by the pre-strain treatment due to difference of modulus of the G/CNC layer and NWF. The G loading dependent sensing range and sensitivity is closely associated with the micro-crack density formed in the G/CNC conductive layer, and the superhydrophobicity of the NWF strain sensor was obtained by dip-coating the Hf-SiO_2/ethanol suspension due to instinct low surface energy and rough microtopography of the Hf-SiO_2 layer. In this work, the

Hf-SiO_2/G/CNC/PDA@NWF strain sensor could achieve a large sensing range of 98% and GF value up to 2.36×10^4 simultaneously. As far as we know, they are the highest values ever reported. Furthermore, the sensor performs excellent waterproofness (WCA = 154°), anti-corrosion ability, outstanding self-cleaning and stability. As a result, the strain sensor can successfully detection various human activities from subtle deformations to vigorous body movements. Specially, the strain sensor also exhibits superior self-cleaning capability and good applicability in humid or underwater harsh outdoor environments.

Acknowledgments

The research was financially supported by National Natural Science Foundation of China (NO: 51803191, 11432003, 11572290), the China Postdoctoral Science Foundation (NO. 2018M642782), the Postdoctoral Research Grant in Henan Province (NO. 001801007), the 111 Project (D18023), and the start-up fund from Zhengzhou University.

Appendix A. Supplementary data

Supplementary data to this article can be found online at https://doi.org/10.1016/j.nanoen.2019.104143.

References

[1] Q. Hua, J. Sun, H. Liu, R. Bao, R. Yu, J. Zhai, C. Pan, Z.L. Wang, Nat. Commun. 9 (2018) 244.
[2] S. Fu, J. Tao, W. Wu, J. Sun, F. Li, J. Li, Z. Huo, Z. Xia, R. Bao, C. Pan, Adv. Mater. Technol. 4 (2019) 1800703.
[3] S. Zhang, H. Liu, S. Yang, X. Shi, D. Zhang, C. Shan, L. Mi, C. Liu, C. Shen, Z. Guo, ACS Appl. Mater. Interfaces 11 (2019) 10922–10932.
[4] J. Li, R. Bao, J. Tao, Y. Peng, C. Pan, J. Mater. Chem. C 6 (2018) 11878–11892.
[5] T. Li, Y. Li, T. Zhang, Acc. Chem. Res. 52 (2019) 288–296.
[6] S. Huang, Y. Liu, Y. Zhao, Z. Ren, C.F. Guo, Adv. Funct. Mater. 29 (2019) 1805924.
[7] J. Tao, R. Bao, X. Wang, Y. Peng, J. Li, S. Fu, C. Pan, Z.L. Wang, Adv. Funct. Mater. 0 (2018) 1806379.
[8] B. Nie, R. Huang, T. Yao, Y. Zhang, Y. Miao, C. Liu, J. Liu, X. Chen, Adv. Funct. Mater. 29 (2019) 1808786.
[9] M. Liu, X. Pu, C. Jiang, T. Liu, X. Huang, L. Chen, C. Du, J. Sun, W. Hu, Z.L. Wang, Adv. Mater. 29 (2017).
[10] W. Wu, H. Haick, Adv. Mater. 0 (2018) 1705024.
[11] R. Bao, C. Wang, L. Dong, R. Yu, K. Zhao, Z.L. Wang, C. Pan, Adv. Funct. Mater. 25 (2015) 2884–2891.
[12] H. Lu, M. Zhang, Y. Yang, Q. Huang, T. Fukuda, Z. Wang, Y. Shen, Nat. Commun. 9 (2018) 3944.
[13] W. Hu, G.Z. Lum, M. Mastrangeli, M. Sitti, Nature 554 (2018) 81.
[14] Y. Yang, L. Shi, Z. Cao, R. Wang, J. Sun, Adv. Funct. Mater. 0 (2019) 1807882.
[15] Y. Qiao, Y. Wang, H. Tian, M. Li, J. Jian, Y. Wei, Y. Tian, D.Y. Wang, Y. Pang, X. Geng, X. Wang, Y. Zhao, H. Wang, N. Deng, M. Jian, Y. Zhang, R. Liang, Y. Yang, T.L. Ren, ACS Nano 12 (2018) 8839–8846.
[16] S. Xinlei, L. Shuiren, S. Yang, L. Jiajie, C. Yongsheng, Adv. Funct. Mater. 28 (2018) 1800850.
[17] G.-J.N. Wang, A. Gasperini, Z. Bao, Adv. Electron. Mater. 4 (2018) 1700429.
[18] X. Li, T. Yang, Y. Yang, J. Zhu, L. Li, F.E. Alam, X. Li, K. Wang, H. Cheng, C.-T. Lin, Y. Fang, H. Zhu, Adv. Funct. Mater. 26 (2016) 1322–1329.
[19] Y. Yu, Y. Luo, A. Guo, L. Yan, Y. Wu, K. Jiang, Q. Li, S. Fan, J. Wang, Nanoscale 9 (2017) 6716–6723.
[20] P. Song, H. Qin, H.L. Gao, H.P. Cong, S.H. Yu, Nat. Commun. 9 (2018) 2786.
[21] H. Liu, M.Y. Dong, W.J. Huang, J.C. Gao, K. Dai, J. Guo, G.Q. Zheng, C.T. Liu, C. Y. Shen, Z.H. Guo, J. Mater. Chem. C 5 (2017) 73–83.
[22] L.-Q. Tao, K.-N. Zhang, H. Tian, Y. Liu, D.-Y. Wang, Y.-Q. Chen, Y. Yang, T.-L. Ren, ACS Nano 11 (2017) 8790–8795.
[23] H. Liu, W.J. Huang, X.R. Yang, K. Dai, G.Q. Zheng, C.T. Liu, C.Y. Shen, X.R. Yan, J. Guo, Z.H. Guo, J. Mater. Chem. C 4 (2016) 4459–4469.
[24] H. Wang, H. Luo, H. Zhou, X. Zhou, X. Zhang, W. Lin, G. Yi, Y. Zhang, Chem. Eng. J. 345 (2018) 452–461.
[25] H. Liu, Q. Li, S. Zhang, R. Yin, X. Liu, Y. He, K. Dai, C. Shan, J. Guo, C. Liu, C. Shen, X. Wang, N. Wang, Z. Wang, R. Wei, Z. Guo, J. Mater. Chem. C 6 (2018) 12121–12141.
[26] Y.L. Wang, Y.Y. Jia, Y.J. Zhou, Y. Wang, G.Q. Zheng, K. Dai, C.T. Liu, C.Y. Shen, J. Mater. Chem. C 6 (2018) 8160–8170.
[27] T. Yang, X. Li, X. Jiang, S. Lin, J. Lao, J. Shi, Z. Zhen, Z. Li, H. Zhu, Mater. Horiz. 3 (2016) 248–255.
[28] H. Liu, J.C. Gao, W.J. Huang, K. Dai, G.Q. Zheng, C.T. Liu, C.Y. Shen, X.R. Yan, J. Guo, Z.H. Guo, Nanoscale 8 (2016) 12977–12989.
[29] S. Wu, R.B. Ladani, J. Zhang, K. Ghorbani, X. Zhang, A.P. Mouritz, A.J. Kinloch, C. H. Wang, ACS Appl. Mater. Interfaces 8 (2016) 24853–24861.
[30] J. Lee, M. Lim, J. Yoon, M.S. Kim, B. Choi, D.M. Kim, D.H. Kim, I. Park, S.-J. Choi, ACS Appl. Mater. Interfaces 9 (2017) 26279–26285.
[31] H. Liu, W.J. Huang, J.C. Gao, K. Dai, G.Q. Zheng, C.T. Liu, C.Y. Shen, X.R. Yan, J. Guo, Z.H. Guo, Appl. Phys. Lett. 108 (2016) 5.
[32] C. Wang, C. Wang, Z. Huang, S. Xu, Adv. Mater. 30 (2018) 1801368.
[33] Q. Li, H. Liu, S. Zhang, D. Zhang, X. Liu, Y. He, L. Mi, J. Zhang, C. Liu, C. Shen, Z. Guo, ACS Appl. Mater. Interfaces 11 (2019) 21904–21914.
[34] H. Liu, Y. Li, K. Dai, G. Zheng, C. Liu, C. Shen, X. Yan, J. Guo, Z. Guo, J. Mater. Chem. C 4 (2016) 157–166.
[35] Y. Hu, H. Zhuo, Z. Chen, K. Wu, Q. Luo, Q. Liu, S. Jing, C. Liu, L. Zhong, R. Sun, X. Peng, ACS Appl. Mater. Interfaces 10 (2018) 40641–40650.
[36] W.J. Huang, K. Dai, Y. Zhai, H. Liu, P.F. Zhan, J.C. Gao, G.Q. Zheng, C.T. Liu, C. Y. Shen, ACS Appl. Mater. Interfaces 9 (2017) 42266–42277.
[37] X. Liao, Z. Zhang, Q. Liao, Q. Liang, Y. Ou, M. Xu, M. Li, G. Zhang, Y. Zhang, Nanoscale 8 (2016) 13025–13032.
[38] K. Yang, F. Yin, D. Xia, H. Peng, J. Yang, W. Yuan, Nanoscale 11 (2019) 9949–9957.
[39] D. Kang, P.V. Pikhitsa, Y.W. Choi, C. Lee, S.S. Shin, L.F. Piao, B. Park, K.Y. Suh, T. I. Kim, M. Choi, Nature 516 (2014) 222–226.
[40] C. Wang, J. Zhao, C. Ma, J. Sun, L. Tian, X. Li, F. Li, X. Han, C. Liu, C. Shen, L. Dong, J. Yang, C. Pan, Nano Energy 34 (2017) 578–585.
[41] X. Su, H. Li, X. Lai, Z. Chen, X. Zeng, ACS Appl. Mater. Interfaces 10 (2018) 10587–10597.
[42] L. Li, Y. Bai, L. Li, S. Wang, T. Zhang, Adv. Mater. 29 (2017) 1702517.
[43] G.M. Ding, W.C. Jiao, L.Y. Chen, M.L. Yan, L.F. Hao, R.G. Wang, J. Mater. Chem. A 6 (2018) 16992–17000.
[44] G.M. Ding, W.C. Jiao, R.G. Wang, Z.M. Chu, Y.F. Huang, J. Mater. Chem. A 7 (2019) 12333–12342.
[45] Z. Li, L. Ye, J. Shen, K. Xie, Y. Li, Compos. Commun. 7 (2018) 23–29.
[46] L. Wang, H. Wang, X.W. Huang, X. Song, M.J. Hu, L.C. Tang, H.G. Xue, J.F. Gao, J. Mater. Chem. A 6 (2018) 24523–24533.
[47] P. Wang, B. Sun, Y. Liang, H. Han, X. Fan, W. Wang, Z. Yang, J. Mater. Chem. A 6 (2018) 10404–10410.
[48] H.-C. Yang, R.Z. Waldman, M.-B. Wu, J. Hou, L. Chen, S.B. Darling, Z.-K. Xu, Adv. Funct. Mater. 28 (2018) 1705327.
[49] P. Wang, M. Chen, H. Han, X. Fan, Q. Liu, J. Wang, J. Mater. Chem. A 4 (2016) 7869–7874.
[50] O. Hitoshi, X. Jing, O. Jun, S. Tetsuo, Langmuir 28 (2012) 4605–4608.
[51] S. Pan, R. Guo, M. Björnmalm, J.J. Richardson, L. Li, C. Peng, N. Bertleff-Zieschang, W. Xu, J. Jiang, F. Caruso, Nat. Mater. 17 (2018) 1040–1047.
[52] D. Zhang, Z. Cheng, H. Kang, J. Yu, Y. Liu, L. Jiang, Angew. Chem., Int. Ed. Engl. 57 (2018) 3701–3705.
[53] Z.-R. Jiang, J. Ge, Y.-X. Zhou, Z.U. Wang, D. Chen, S.-H. Yu, H.-L. Jiang, NPG Asia Mater. 8 (2016) e253.
[54] M. Liu, S. Wang, L. Jiang, Nat. Rev. Mater. 2 (2017) 17036.
[55] L. Zhang, H. Li, X. Lai, T. Gao, J. Yang, X. Zeng, ACS Appl. Mater. Interfaces 10 (2018) 41784–41792.
[56] G. Li, K. Dai, M. Ren, Y. Wang, G. Zheng, C. Liu, C. Shen, J. Mater. Chem. C 6 (2018) 6575–6583.
[57] J.H. Pu, X.J. Zha, L.S. Tang, L. Bai, R.Y. Bao, Z.Y. Liu, M.B. Yang, W. Yang, ACS Appl. Mater. Interfaces 10 (2018) 40880–40889.
[58] G. Shi, Z. Zhao, J.-H. Pai, I. Lee, L. Zhang, C. Stevenson, K. Ishara, R. Zhang, H. Zhu, J. Ma, Adv. Funct. Mater. 26 (2016) 7614–7625.
[59] W. Liu, M.-S. Song, B. Kong, Y. Cui, Adv. Mater. 29 (2017) 1603436.
[60] Z. Lou, L. Li, L. Wang, G. Shen, Small 13 (2017) 1701791.
[61] S. Wu, S. Peng, Z.J. Han, H. Zhu, C.H. Wang, ACS Appl. Mater. Interfaces 10 (2018) 36312–36322.
[62] Y. Lin, S. Liu, S. Chen, Y. Wei, X. Dong, L. Liu, J. Mater. Chem. C 4 (2016) 6345–6352.
[63] Z. Zeng, S.I. Seyed Shahabadi, B. Che, Y. Zhang, C. Zhao, X. Lu, Nanoscale 9 (2017) 17396–17404.

Dr Hu Liu, an Associate Professor of National Engineering Research Center for Advanced Polymer Processing Technology of Zhengzhou University, obtained his PhD from Zhengzhou University (2017), and worked as a joint PhD student with Prof. Zhanhu Guo at University of Tennessee, Knoxville, sponsored by China Scholarship Council (2015–2016). His current research interest focuses on the multifunctional polymer based nanocomposites, especially the conductive polymer composites based sensor, electromagnetic shielding materials and thermal insulating aerogel.

Mr Qianming Li, currently a Master student at the National Engineering Research Center for Advanced Polymer Processing Technology of Zhengzhou university, obtained a BE degree in College of Chemical Engineering and Pharmaceutics from Henan University of Science and Technology (2018). His research interests focus on multifunctional polymer nanocomposites for strain sensors and superhydrophobic applications.

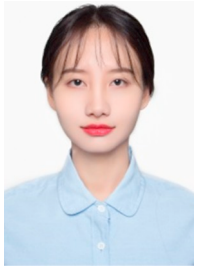

Miss Yibing Bu, currently a Master degree candidate in National Engineering Research Center for Advanced Polymer Processing Technology of Zhengzhou University, obtained her bachelor degree in Materials Science and Engineering at China University of Geosciences, Wuhan, China (2019). Her research interests focus on multifunctional polymer nano-composites for wearable electronic sensors.

Dr Na Zhang, an Associate Professor of National Engineering Research Center for Advanced Polymer Processing Technology of Zhengzhou University, obtained her PhD from Zhengzhou University (2013), and worked as a joint PhD student with Prof. L James Lee at The Ohio State University, Ohio, sponsored by China Scholarship Council (2010–2012). Her current research interest focuses on solid particle erosion resistance of thermoplastic and thermoset composite, especially the polymer composites with blades, wings and lightweight cars.

Dr. Chunfeng Wang received his B.S. degree in materials science and engineering from Zhengzhou University in 2013, and his Ph.D. degree in materials processing engineering from Zhengzhou University in 2019. He is currently a research associate professor in College of Physics and Optoelectronic Engineering, Shenzhen University. His research interests include stretchable electronics and energy materials.

Prof. Caofeng Pan received his B.S. degree (2005) and Ph.D. degree (2010) in Materials Science and Engineering from the Tsinghua University, China. He then joined the group of Prof. Zhong Lin Wang at the Georgia Institute of Technology as a postdoctoral fellow from 2010 to 2013. He is currently a professor and a group leader at the Beijing Institute of Nanoenergy and Nanosystems, Chinese Academy of Sciences. His research interests mainly focus on the fields of piezotronics/piezophototronics for fabricating new electronic and optoelectronic devices, nanopower source, hybrid nanogenerators, and self-powered nanosystems. Details can be found at http://www.piezotronics.cn/.

Prof. Liwei Mi received his B.S., M.S. and Ph.D. from Zhengzhou University. In 2014, he worked as a professor of materials science in Zhongyuan University of Technology. His current research interest focuses on the controllable preparation and performance study of functionalized micro/nanomaterials. He has published over 110 peer-reviewed articles and holds 15 authorized invention patents of China.

Prof. Zhanhu Guo, an Associate Professor in the Department of Chemical and Biomolecular Engineering, University of Tennessee, Knoxville, USA, obtained a PhD degree in Chemical Engineering from Louisiana State University (2005) and received three-year (2005–2008) postdoctoral training from the Mechanical and Aerospace Engineering Department at the University of California Los Angeles. Dr Guo chaired the Composite Division of the American Institute of Chemical Engineers (AIChE, 2010–2011) and directs the Integrated Composites Laboratory. His current research focuses on multifunctional nanocomposites for education, transportation, safety, information, catalysis, energy harvesting and storage, electronics and environmental remediation applications.

Prof. Chuntai Liu, currently a Professor of the National Engineering Research Center for Advanced Polymer Processing Technology (NERC) of Zhengzhou University, obtained his PhD from Zhengzhou University (2003), and worked as a visiting scholar at the Ohio State University (2006–2007). He serves as the deputy director of NERC of Zhengzhou University. His research focuses on multifunctional polymer composites including processing-microstructure-properties.

Prof. Changyu Shen, currently a professor of the National Engineering Research Center for Advanced Polymer Processing Technology (NERC) of Zhengzhou University and an academician of Chinese Academy of Sciences, obtained his M.S. and Ph.D. from Dalian University of Technology in 1987 and 1990 respectively. Shen has made original and innovative contributions to numerical simulation of plastic forming process, optimization design and manufacture of plastic mold as well as structured and lightweight composites. He now serves as the director of NERC of Zhengzhou University.